Eur. Phys. J. Special Topics **229**, 1881–1896 (2020)

https://doi.org/10.1140/epjst/e2020-900273-x

THE EUROPEAN PHYSICAL JOURNAL SPECIAL TOPICS

Regular Article

Delay of ice formation on penguin feathers*

Elaheh Alizadeh-Birjandi[1], Faryar Tavakoli-Dastjerdi[1], Judy St. Leger[2], Kym F. Faull[3], Stephen H. Davis[4], Jonathan P. Rothstein[5], and H. Pirouz Kavehpour[1,a]

[1] Department of Mechanical and Aerospace Engineering, UCLA, Los Angeles, CA, USA
[2] SeaWorld Parks and Entertainment, San Diego, USA
[3] Department of Psychiatry and Biobehavioral Sciences, UCLA, Los Angeles, CA, USA
[4] Department of Engineering Sciences and Applied Mathematics, Northwestern University, Evanston, IL, USA
[5] Department of Mechanical and Industrial Engineering, University of Massachusetts, Amherst, MA, USA

Received 1 December 2019 / Accepted 23 July 2020
Published online 14 September 2020

Abstract. Cold-weather penguins continually dive in and out of the water and get splashed by waves during the frigid Antarctic winter. Yet, even under these extreme sub-zero conditions, macroscopic ice crystals are typically not observed on their feathers. In this work, we hypothesize that the origin of the anti-icing properties of a cold-weather penguin's feathers comes from a unique combination of the feather's macroscopic structure, the nanoscale topography of its barbules, and the hydrophobicity of its preen oil. We show that, the combination of all three, make cold-weather penguin feathers both highly water repellant and icephobic. In this paper, we present the results from a series of droplet freezing experiments performed on feathers from a number of species of both cold-weather and warm-weather penguins. Compared to a smooth glass substrate, freezing was delayed by a factor of 30-times for drops deposited on warm-weather penguin feathers and 60-times for cold-weather penguins. The difference in freezing time between warm- and cold-weather penguins was statistically significant and can be attributed to the increase in the contact angle measured between the drop and the feather of the cold-weather penguin. This increased contact angle is the result of an increase in the hydrophobicity of the preen oil and the inclusion of nanoscale, air-trapping dimples on the surface of the barbules. The physics of this delay are explained through the development of a simple heat transfer model which demonstrates that increasing contact angle is a primary cause of increased freezing time and icephobicity. The results of this study can be used to motivate the designs of biomimetic surfaces to minimize ice formation in extreme conditions for a number of important engineering applications.

* Supplementary material in the form of one pdf file available from the Journal web page at https://doi.org/10.1140/epjst/e2020-900273-x.

[a] e-mail: pirouz@seas.ucla.edu

1 Introduction

Penguins are flightless birds living in diverse geographical locations in the southern hemisphere. Humboldt penguins live in temperate zones near the equator whereas circumpolar species like the Gentoo, Macaroni, Emperor, and Adelie have adapted to the extreme cold in Antarctic regions, where air temperatures may reach −40 °C with wind speeds of 40 m/s and water temperatures around −2.2 °C [1,2]. Penguins jump in and out of the water every day. Yet, no macroscopic ice formation can be observed on their feathers in nature or in captivity even on the coldest days of the year. A better understanding of the origins of the amazing anti-icing ability of Antarctic penguins could help address one of the major challenges in the aerospace industry, ice formation and buildup on the surface of aircraft wings.

The results of numerous experimental studies have shown that even a very small amount of ice accumulation at critical locations on an aircraft can have a negative impact on its performance [3]. Some of the observed effects include: substantial decrease in lifting capability, frequent control-surface anomalies, increase in drag, malfunctioning of sensors, and probes, and, in some cases, reduction in engine performance and stability [4,5]. Ground-based de-icing is both expensive and time consuming. In this method, a mixture of chemicals is heated and sprayed under pressure to remove ice on the aircraft. The toxicity of the deicing fluids is also an environmental concern [5,6]. The development of surfaces that can resist icing both on the ground and in flight is therefore a significant advantage for both commercial and military aircraft. Ice accumulation can also reduce the performance of other lifting surfaces such as the blades of wind turbines by changing the aerodynamic profile of the blades and adding to the operational loading of the entire rotor, which can lead to significant energy loss and reduction of power production [7,8]. Current de-icing methods require the turbine to be stopped or use power from the turbine itself which decreases the efficiency of the system [9,10]. A number of strategies have been developed in the past to find suitable materials to delay or prevent ice formation [11–16], all with limited success.

In this paper, we turn our attention to nature and the anti-icing property of Antarctic penguins for inspiration in the development of novel and efficient ice-phobic surfaces. We also demonstrate that penguin ice-resisting ability is the product of a unique combination of surface chemistry, the physical structure of the penguin feathers, and a heat transfer mechanism directly related to contact angle. Through a theoretical and experimental study of ice formation on the feathers of a series of different penguins, we show that cold-weather penguin feathers are more ice-resistant than those of warm-weather penguins due to differences in both the surface chemistry and fine structure of the feathers. The results are extended to superhydrophobic surfaces in general through the development of a heat-transfer model that explains the primary mechanism behind the delay of solidification on water-repellent materials. It should be noted that the main concern of this work is to prevent the initiation of freezing as when the trijunction starts solidifying, the drop adheres to the surface, and it becomes almost impossible for the drop to roll off of the surface under normal circumstances.

2 Materials and methods

2.1 Experimental procedure

A series of experiments were performed to observe the rate at which water droplets freeze on penguin feathers. For these experiments, five different types of penguins

have been used, and the list from cold to warm-weather habitat includes Adelie and Emperor, which are endemic to Antarctica, Gentoo and Macaroni that reside in sub-Antarctic regions, and finally Humboldt, which is a South American penguin. Feathers were placed inside the drop shape analyzer, Krüss DSA 100, and cooled to $T = -20\,℃$. This instrument was used for recording the droplet spreading dynamics and solidification process and provided accurate measurement of the dynamic contact angle and contact diameter of the droplet. The contact angle measurements are performed for single droplet on both individual feathers and a packed group of feathers. Liquid water drops at room temperature were then deposited on the penguin feathers. The volume of drop was set to $5\,\mu$l for all the experiments in order to make sure the results are consistent, and the size of the droplet was small enough to neglect the gravitational effects. In this device, the temperature of the solid targets can be adjusted by a Peltier element situated inside, the droplet placed on the cold substrate was illuminated from one side, and a high-speed camera captured images continuously during solidification which was used in real-time monitoring of the process. All the experiments were performed inside the environmental chamber with controlled humidity to prevent the effect of condensation and frosting. For comparison, water was also deposited on a smooth glass substrate, which was rinsed successively in ethanol, methanol, and deionized water.

It should be noted that in these experiments, the temperature of the feathers is well chosen after comprehensive research to fit penguins natural living conditions and provide relevant results, and there are two main reasons behind the constant temperature of $-20\,°\mathrm{C}$. First, the temperature of the outside of the body of the penguins is almost the same as outside air in their natural habitat [17] because otherwise their survival would be impossible due to the severe heat loss. Second, at this temperature, the nucleation activation energy barrier is minimized and delay in the onset of freezing is mostly the result of a reduced heat transfer due to geometric effects as described below.

2.2 Data analysis

In this study, 65 samples were obtained from 5 different types of penguin feathers under the same experimental conditions. To compare the values and acquire a relationship between the freezing delay times on different species of penguins, the average values and standard error were calculated. The analysis of variance (ANOVA) was used to analyze the difference among the groups applying the significance level of $p < 0.01$, and the results show that the average values for cold weather penguins (Adelie, Emperor, Gentoo, and Macaroni) are statistically different than the warm weather penguin (Humboldt) (Fig. 2b, caption).

3 Contact angle measurements and freezing experiments on penguin feathers

In Figure 1, the equilibrium contact angles of water droplets on various penguin feathers are shown at room temperature. The results are interesting in that the feathers of penguins in colder environments always have higher contact angle with water than do warm-weather penguins. This observation suggests there might be a direct relationship between the contact angle and the penguins' habitat. Our hypothesis is that Antarctic penguins have evolved, in part, to improve their anti-icing properties. In order to quantify and compare penguins' ice-resisting abilities, we have performed a number of freezing experiments on different penguin feathers and measured the time of icing initiation.

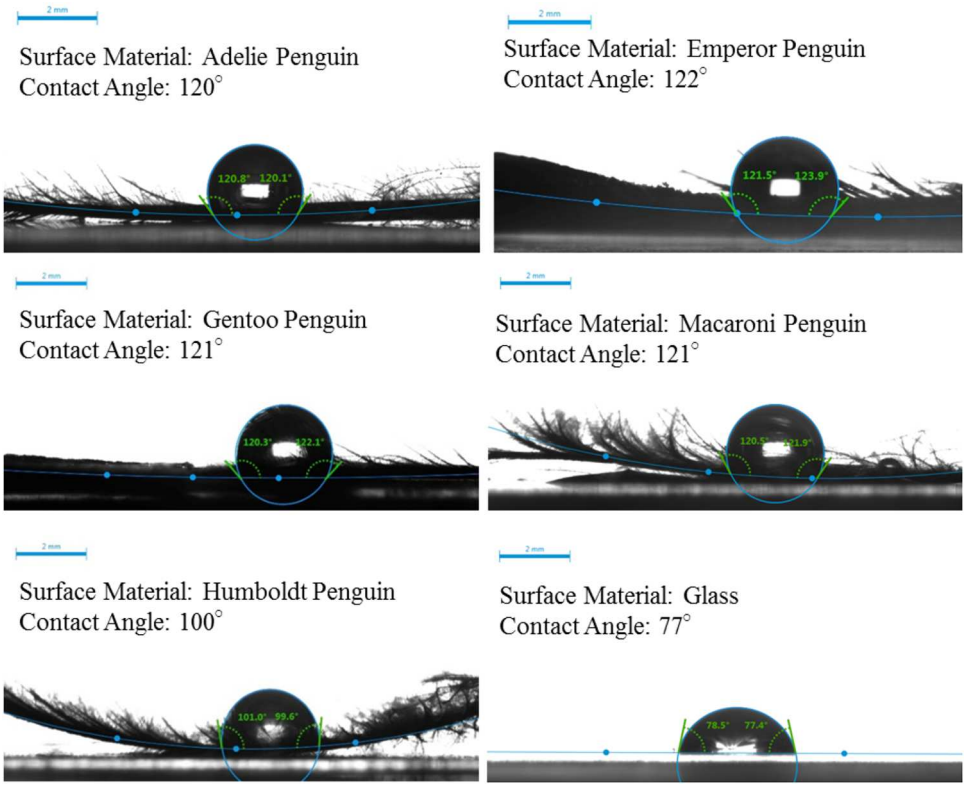

Fig. 1. Static contact-angle measurements on penguin feathers. The contact-angles for water droplets on different penguin feathers and a glass substrate are measured using the ellipse fitting method [18]. The reported values on the figure are the roundup average contact angles, and the exact numbers are: Adelie 119.4 (±1.6)°, Emperor 121.2 (±1.2)°, Gentoo 120.3 (±1.8)°, Macaroni 120.7 (±2.2)°, and Humboldt 99.1 (±4.1)°.

A series of images showing the freezing process on a cold-weather penguin feather (Adelie), a warm-weather penguin feather (Humboldt), and a clean, smooth glass substrate is presented in Figure 2a. In this experiment, the water drop at room temperature with the volume of 5 μl is deposited on each surface at −20 °C. On the glass substrate, the water drop begins to solidify roughly one second after the start of the experiment. The heterogeneous nucleation and growth of ice from the glass substrate progresses vertically through the drop and resulting in a pointed frozen droplet shape at the end of freezing process consistent with the work of Anderson et al. [19]. Under the same conditions, when a water droplet is placed on a warm-weather Humboldt penguin feather, the solidification process is delayed considerably and ice crystals are observed to grow everywhere at once resulting in a nearly-instantaneous uniform increase in the opacity of the drop. As shown in Figure 2a, the onset of the solidification process on a Humboldt penguin feather is 30 s after the droplet deposition. Even more interesting, for a water droplet deposited on a cold-weather Adelie feather, the freezing does not begin until 57 s after droplet deposition as shown in Figure 2a. The result is roughly a 60-fold increase in the solidification initiation time on an Adelie feather when compared to the glass substrate and a 2-fold increase when compared to the Humboldt feather.

The same set of experiments was carried out for several examples of warm-weather and cold-weather penguin feathers and the results are presented in Figure 2b.

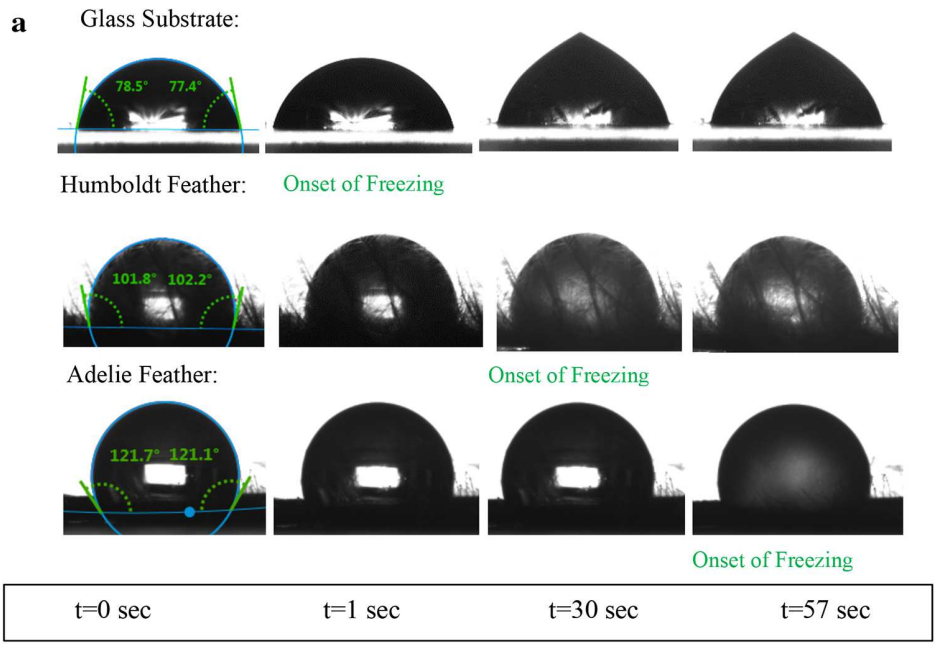

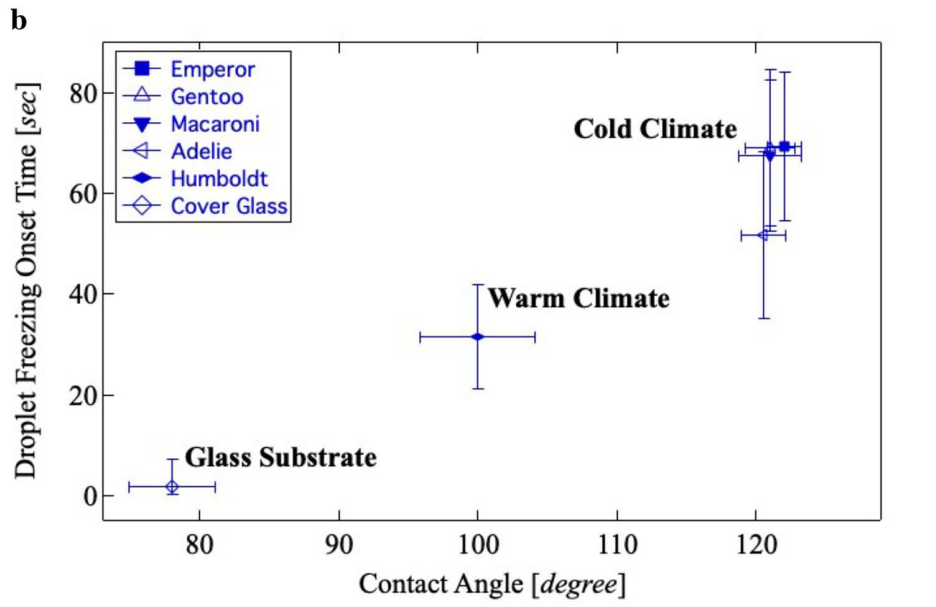

Fig. 2. Freezing experiments on penguin feathers. (a) Video sequence of water freezing on different substrates at $-20\,^{\circ}\mathrm{C}$. The droplets were deposited on the solid target with the flow rate of 2 ml/min and total volume of 5 μl. The elapsed times are 0, 1, 30, and 57 s, respectively. (b) Time required for the onset of droplet freezing as a function of contact angle for a 5 μl water drop on a series of penguin feathers in an environmental chamber cooled to $T = -20\,^{\circ}\mathrm{C}$. There are significant differences between the freezing delay time of cold-weather penguins (Adelie, Emperor, Gentoo, and Macaroni) and the warm-weather one (Humboldt) ($F(4, 60) = 4.406$, $p = 0.00345$). For comparison, the onset time of freezing for a droplet on a smooth glass substrate with a contact angle of 75° was found to be close to one second.

Depending on where a penguin resides, these results clearly show that the water-repellency and anti-icing characteristics of the penguin's feathers can be quite different. The change in wettability appears to make cold-weather penguin feathers better suited for forestalling ice formation and for keeping the penguins free of ice even in the harshest climates on earth. It should be noted that although large contact angles appear to delay the solidification process, it is not the sole factor governing the ice formation. For instance, the feathers of Adelie penguins are less ice-resistant compared to other cold-weather penguins even though their contact angles are comparable. Other factors such as the presence of an insulating air layer beneath the droplet, the reduction of the effective contact area of the drop, the abundance of nucleation sites, and the details of the surface microstructure can therefore have an effect, which is discussed in the Supporting Information (SI) section.

4 Feather structure analyses

Feathers are the most prominent, complex, and varied integumentary derivatives of birds. The basic plan of a penguin feather consists of a shaft with regularly spaced branches on either side. The branches, called barbs, form interconnected sheets or vanes which are the most visible part of a feather. A barb repeats most of this plan, having a central axis with tightly spaced barbules on either side. Although there have been many studies on morphology and structure of bird feathers [20–22], none of them has studied the nano-size pattern on penguin feathers that makes them excellent ice-repellent surfaces. To determine the important parameter making penguin feathers ice-phobic, it is essential to analyze the feather structure of penguins living in diverse environmental conditions. Therefore, a series of SEM (scanning electron microscopy) images of feathers of three different penguins were taken as shown in Figure 3. The SEM images in Figure 3a reveal the micron-scale features of the Emperor penguin feathers. In this figure, the barbs and barbules are clearly visible with the barbs roughly 20 μm in diameter and spaced 300 μm apart with a dense array of barbules less than 5 μm in diameter protruding from the side of each barb. A further increase in the magnification shows the hooks branching from the barbules and the microstructure along the surface of the barbules creating a hierarchical structure enhancing the non-wetting properties of the feathers.

A closer look at the feathers is presented in Figure 3b. These images reveal an extremely fine structure along the surface of the shaft which appears to be a series of dimples and cavities. For the cold weather Gentoo penguin feather, the surface features are found to be in the range of 80–260 nm in diameter with average of 174 nm and population density of $4.02/\mu m^2$. The highly packed structure and complex nano-texture of the feathers provide the roughness necessary to trap air between and along the barbules, the barbs, and the shaft making the feathers naturally hydrophobic [23]. However, for the warm weather penguin, Humboldt, these features are slightly different. The surface patterns are larger in size, smaller in depth, and more dispersed. The diameter of the surface features for Humboldt feather is between 350 and 600 nm with the average size of 462 nm and population density of $1.01/\mu m^2$. These features also help increase the water droplet contact angle on Humboldt feather although, as seen in Figure 2, the warm-weather feather's contact angle is 20° less than the best cold-weather feathers. It should be noted that this is the first time these nano-structures are observed on the penguin feathers. The work done by Wang et al. [24] is the only previous study on icephobicity of penguin feathers and their potential to provide a passive anti-icing system. However, the only type of penguin studied was the Humboldt, the warm-weather penguin, and no such nano-structures were reported.

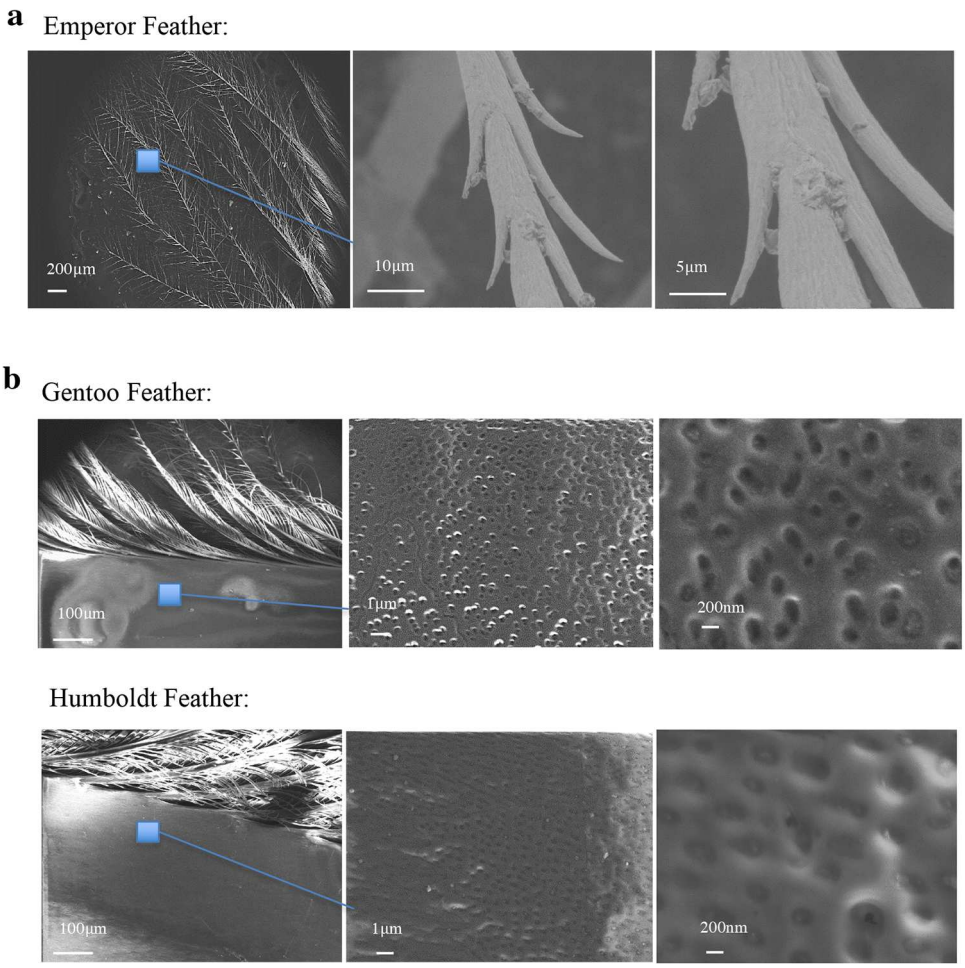

Fig. 3. Feather structure analysis. (a) The SEM pictures of the surface of the barbules of the Emperor penguin feather. The pictures show the hooks branching from the barbules and also the micro-texture along their surface. (b) SEM images of feathers of the Gentoo and Humboldt feathers with three different magnifications to observe the submicron size air cavities on the shaft surface at three different magnifications increasing from left to right.

In addition to their surface structure, feathers have a unique surface chemistry. They are made of keratin, which has a critical surface tension of ≈20 dyn/cm [25] and are covered by preen oil produced *via* the uropygial gland located at the base of the penguins tail [26]. Penguins cover the surface of their feathers with preen oil sometimes several times a day. The chemical composition of preen oil is primarily monoester waxes with fewer triglycerides and hydrocarbons [27].

To examine the preen oil composition and abundance on different penguin feathers in nature and subject to the experiment, a complete gas chromatography/mass spectrometry (GC/MS) analysis is performed and the details are presented in SI section. The GC/MS analysis reveals that both samples subject to the experiment and the control group, freshly collected feathers, have a similar profile, and the intensities of the components are in close proximity. A comparison between preen oil composition of different penguins was also performed by Jacob [2], and it was shown that the chemical compositions of preen-oil vary with species. He studied the preen waxes of

three species of penguins and showed that preen-oil compositions of penguins have two different wax patterns; the cold-weather penguins like the Gentoo and rock-hopper penguins contain mostly 3-methyl-branched acids; however, the warm-weather penguins like the Magellanic penguin contains primarily 2- and 4-methyl-substituted fatty acids. It is believed that preen oil has many functions including protecting keratin, providing antibacterial properties, acting as an odorant, as well as improving the non-wetting properties of the feathers by reducing their surface energy and increasing their contact angle with water. Jacob's results show that depending on where penguins reside, the preen oil composition and consequently the water-repellency characteristics of these penguins are extremely different with the preen oil of cold weather penguins being more hydrophobic [2].

It is clear that both the feather surface nano-structures and the preen oil composition depend the habitat of the penguin species and that the feathers with the highest contact angle with water are found amongst the many species of cold-weather penguins.

5 Theoretical modeling of heat transfer on superhydrophobic surfaces

The combination of the hierarchical structure of the feathers along with low critical surface tension of keratin and preen oil in these birds increases their contact-angle with water and reduces their contact-angle hysteresis making the feathers hydrophobic [28,29]. A number of different theories have been proposed to explain the significant delay in the solidification time of water drops and the reduction of the adhesion strength of the incipient ice formation on hydrophobic and superhydrophobic surfaces [11,13,15,30–32]. Nonetheless, the underlying mechanism of the icephobicity of hydrophobic and superhydrophobic surfaces is still debated [12,31,33–38].

Quéré and his coworkers believe that on hydrophobic surfaces, a droplet sits on a composite surface of air and solid, and the presence of this insulating trapped air layer reduces the adhesion and delays the freezing process by slowing the rate of heat transfer [39]. Another study of icing behavior of superhydrophobic surfaces has been done by Alizadeh et al. [40]. They showed that the icing delay on superhydrophobic surfaces could be due to the lower probability of heterogeneous nucleation and the reduction of water-solid interfacial area. Although some of these factors are likely to be effective, the dominant physical mechanism that governs the anti-icing properties of hydrophobic and superhydrophobic surfaces in general and penguin feathers in particular is subject to some controversy.

Based on our experimental results, we believe that there is a strong correlation between the start of freezing and contact angle. Our hypothesis is that, for droplets on penguin feathers and other high contact angle surfaces, there is a further delay in solidification resulting from a geometrical constraint on the heat flow. In other words, as the contact angle of the droplet increases above 90°, the curvature and shape of the isotherms change (see Fig. 4) confining the conduction heat flow to a smaller surface. We also believe that this is the most dominant factor in the delay of onset of freezing, and a brief discussion on quantitative comparison between different factors is presented in SI section.

To test our hypothesis, an approximate theoretical heat-transfer model was developed. In this model, we do not explicitly investigate phase change. Instead, we interrogate the resulting temperature fields to determine when sufficient supercooling has been achieved in the water droplets to initiate the nucleation of crystals. In our model, the water droplet with initial temperature of T_0 was approximated as a

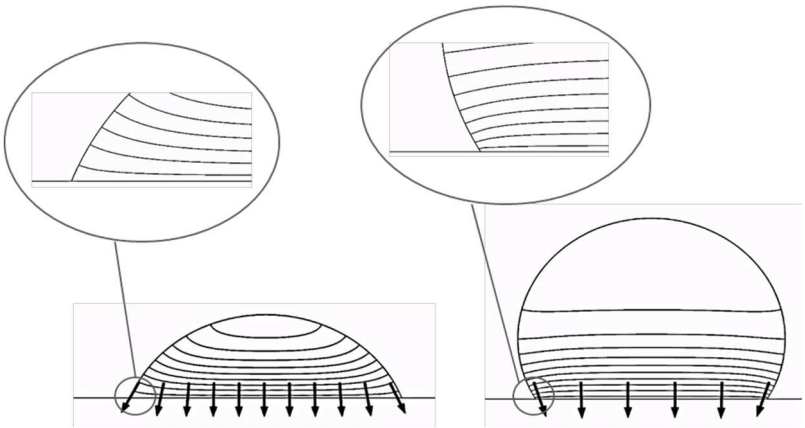

Fig. 4. Isotherms propagation inside droplets on hydrophilic and hydrophobic surfaces. Schematic diagram of isothermal lines on droplets of contact angle smaller (left) and larger (right) than 90°.

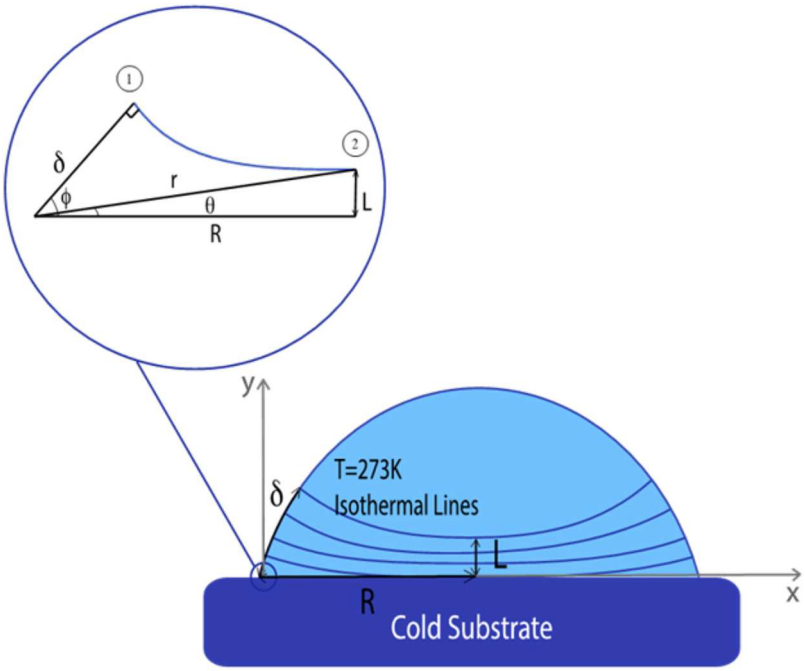

Fig. 5. Geometrical parameters near the contact-line. Growth of isotherms on a droplet placed on cold solid surface.

spherical cap with radius R and contact-angle φ as appeared in Figure 5. The change in surface temperature, T_w, and convective heat losses to the air were assumed to be negligible.

We should discuss the assumption of wall temperature to be constant and equal to wall temperature here. For feathers, the value of thermal effusivity, $(k\rho c_p)^{1/2}$, the product of thermal conductivity, k, density, ρ, and heat capacity, c_p, is approximately one-third that of water. As a result, the interface temperature between the droplet

and the substrate will be closer to the temperature of the water than the surface. By assuming the interface temperature to equal to the substrate temperature, we are considering the worst-case scenario for droplet freezing as we are using an interface temperature that is colder than what is actually experienced during the experiments.

To obtain the onset time of freezing, the observable growth of the isotherms at the liquid–air interface, δ, was calculated as shown in Figure 5. In the vicinity of the contact line, the quasi-steady two-dimensional heat transfer equation in a wedge [41] was solved to determine the temperature field and surface heat flux near the contact-line. The rationale is that the diffusion time scale near the contact line is much shorter than the solidification time and hence a quasi-steady assumption is justifiable. Following series of papers by Davis and co-workers (e.g., [41]), due to the absence of fluid flow, the energy equation can be written as $\partial T/\partial t = \alpha\, \nabla^2 T$ where α is the thermal diffusivity. In dimensionless form, this becomes $\partial \overline{T}/\partial \overline{t} = \frac{\alpha t_0}{\delta^2}\, \overline{\nabla}^2 \overline{T}$. The dimensionless pre-factor $\alpha t_0/\delta^2$ is much larger than one for the case of water. Therefore, Anderson and Davis [41] showed that one can solve a quasi-steady conduction near the contact line to obtain the shape of the temperature distribution there.

Now, we focus at the line perpendicular to the substrate and at the center of the droplet. This is the location of symmetry for all of isotherms at every time, which makes it a very useful for our approximation. At this symmetry line, change of temperature with time is identical to semi-infinite body, $L(t) \approx \sqrt{\alpha t}$. Therefore, as a given temperature moves in this line with time, the entire isotherm corresponding to that temperature moves with it. In our theoretical work, we have combined these two approximations to find the onset of solidification near the contact line.

In order to obtain the movement of the isotherms with time, we recognize that the point on the isotherm at the center of drop follows thermal diffusion principals for semi-infinite body. From these assumptions, the time evolution of these constant temperature lines can be estimated.

Under these conditions, the heat transfer equation simplifies to the Laplace's equation:

$$\nabla^2 T = 0 \tag{1}$$

The local general solution of equation (1) in polar coordinates was found as follows [42]:

$$T(r,\theta) = r^{\tau}\left[A\cos(\tau\theta) + B\sin(\tau\theta)\right] + C\theta + D, \tag{2}$$

where τ, A, B, C, and D are constants of integration. The temperature at the wall was fixed ($\theta = 0,\ T = T_w$) and the air/liquid interface was assumed to be a perfect insulator (i.e., heat loss at the edge is negligible, $\theta = \varphi,\ \partial T/\partial\theta = 0$). Therefore, the resulting temperature profile within the drop becomes:

$$T\,(r,\theta) = T_w + Br^{\tau}\sin(\tau\theta) \quad \tau = \frac{(m+1/2)\,\pi}{\varphi} \quad m = 0,1,2,\ldots \tag{3}$$

Equation (3) is the solution for the steady heat transfer in a wedge. However, we need to obtain the time-dependent temperature profile to determine whether or not the onset of freezing is delayed. Because of the symmetry, it is reasonable to assume that at the centerline, the supercooling process is not affected by the presence of a contact-line. Thus, the heat flux and temperature gradient on the centerline were obtained using the unsteady one-dimensional heat conduction equation (i.e., the centerline acts as a part of a semi-infinite body). As shown in Figure 5, points

(1) and (2) lie on the same isotherm, i.e., $T_1 = T_2$. As a result,

$$T_w + Br_1^{\tau}\sin(\tau\theta_1) = T_w + Br_2^{\tau}\sin(\tau\theta_2). \tag{4}$$

Considering the polar coordinates of points (1) and (2), $(r_1 = \delta,\ \theta_1 = \varphi)$ and $(r_2 = r, \theta_2 = \theta)$, equation (4) can be rewritten as

$$\delta^{\tau}\sin(\tau\varphi) = r^{\tau}\sin(\tau\theta). \tag{5}$$

The heat conduction equation for a semi-infinite body indicates that the thermal penetration depth is proportional to $\sqrt{\alpha t}$, where α is the thermal diffusivity. Based on the geometry presented in Figure 5, $r = \sqrt{L^2 + R^2}$, where $L \approx \sqrt{\alpha t}$ and R is the contact radius of the droplet. Using non-dimensional time-scales and length-scales ($\eta = \alpha t/R^2$, which is the Fourier number, and δ/R respectively), the dimensionless location of different isotherms can be obtained as a function of time and contact angle

$$\frac{\delta}{R} = \sqrt{\eta + 1}\left(\sin\frac{(m + 1/2)\,\pi\tan^{-1}\sqrt{\eta}}{\varphi}\right)^{\frac{\varphi}{(m+1/2)\pi}}. \tag{6}$$

In Figure 6, the variations of the dimensionless location on the surface of the drop, δ/R, of the freezing point isotherm at $T = 0\,^{\circ}\mathrm{C}$ is presented for several different contact angles as a function of dimensionless time, η. Here, $\delta/R = 0$ corresponds to the location of the freezing point isotherm at the contact-line. The three contact angle values in Figure 6 (70°, 100°, and 120°) correspond to the contact angle of water droplet on glass, on a Humboldt feather, and on an Adelie feather, respectively. The freezing point isotherm at the liquid–air interface progresses more slowly up the drop with increasing contact angle. This observation demonstrates a strong correlation between the contact angle and the rate of drop cooling. It also implies that the onset of solidification for droplets on surfaces with large contact angles is delayed as the fluid must first be supercooled well below zero before nucleation of ice crystals can occur.

Nucleation rate can also affect the freezing time. To understand whether nucleation rate effects are a primary or secondary cause of the observed freezing time delay, the nucleation time was approximated for the glass surface and both the cold-weather and warm-weather penguins. The nucleation time can be approximated as

$$t_n \approx \frac{1}{JA\ (1 - \Phi)}, \tag{7}$$

where J is the rate of nucleation per unit area, A is the wetted surface area under the drop which we assume can be approximated by a truncated sphere, and Φ is the porosity of the surface. The porosity of the glass is $\Phi = 0$ and the porosity of the feathers can be approximated from the contact angle of water on the feathers assuming that $\theta = (1 - \Phi)\,\theta_{preen} + \Phi(180^{\circ})$. For the cold-weather penguins $\Phi \sim 30\%$, while for warm weather penguins $\Phi \sim 10\%$. Thus, if we assume that the nucleation rate is the same for all three cases, a delay of $\sim 2\times$ is expected for the warm-weather penguin feather compared to glass and $\sim 5\times$ for the cold-weather penguin feather compared to glass. These values are clearly much less than was observed experimentally ($\sim 15\times$ and $35\times$ respectively). As a result, it can be concluded that for feathers, the reduction in the rate of droplet cooling is the primary cause of the observed freezing time delay and not the reduction in nucleation sites associated with increased contact angle.

For further comparison to the experiments, a dashed line on Figure 6 is drawn across the data at $\delta/R = 0.2$. This is the location within the images of Figure 2

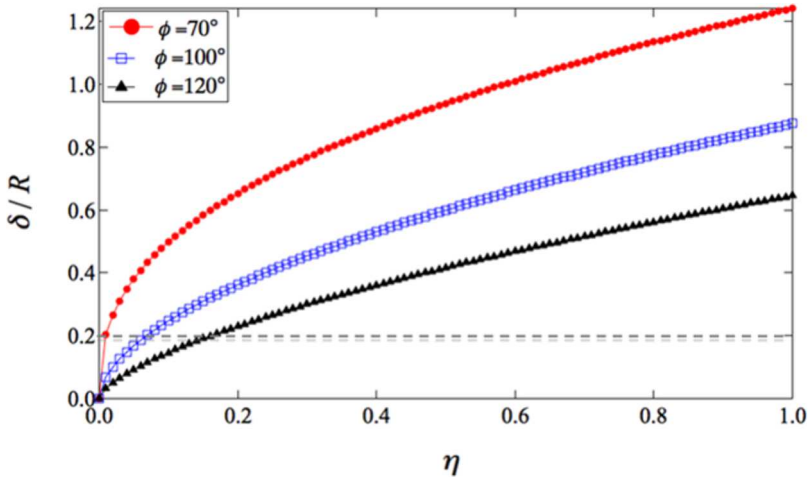

Fig. 6. Theoretical modeling of heat transfer through the droplet of different contact angle. Progression of solidified layer at the edge of the droplet versus time for surfaces of different contact angle from hydrophilic to superhydrophobic. $\delta = 0$ corresponds to the surface of the substrate. At a constant time, the solidified layer ascended less along the drop's liquid–gas interface for drops of higher contact angle.

where the freezing front in the drop first becomes clearly observable for the case of the glass substrate. Comparison of the time delay in the freezing onset using the values obtained from the theoretical model (Fig. 6) and the experimental data (Fig. 2) shows good agreement between the model and experiment. The time delay for the freezing point isotherm to reach $\delta/R = 0.2$ for cold weather penguin feathers was 2.5 times more than the warm weather penguin feather based on the analytical model. From the experimental data, the ratio of average freezing time delay for cold weather penguin feather to warm weather penguin feather was 2.1 times.

It should be noted that the model is intended to verify the effect of contact angle and change in the profile of isotherms on the delay of freezing initiation and show the overall trend on how these two phenomena are related. As explained in the SI section, the small discrepancy between the model and experiment is primarily because in the theory, the temperature at the wall is taken to be constant in order to solve the heat transfer equation analytically. However, in reality, the temperature of the solid is slowly changing, which affects the onset time of freezing.

6 Numerical simulation

A set of numerical simulations was carried out with COMSOL Multiphysics to obtain the determining factors in the time delay of onset of freezing and to corroborate our experimental and analytical studies. In these simulations, three different water drops with initial temperature of 300 K were placed on a glass substrate at an initial temperature of 250 K. Temperature profiles one second after droplet deposition are presented in Figure 7. As in the analytical work in the previous section, phase change was not considered in this model. Droplet A had the same contact area with the solid surface as Droplet B but the contact angle was smaller than 90°. As shown in Figure 5, the freezing-point isotherm was found to advance further into the droplet with the lower contact angle. A third droplet, Droplet C, was also studied. Droplet C had the same contact angle as Droplet B, but a smaller contact area with the substrate.

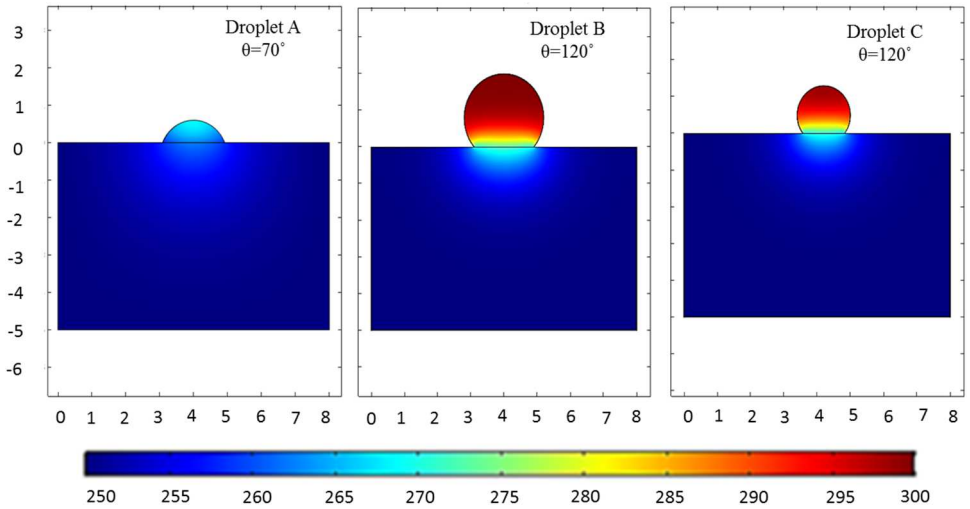

Fig. 7. Heat-transfer simulations for water droplets at 300 K for drops with different contact angles and contact areas on a surface with temperature at 250 K at $t = 1$ s. Droplets A and B have the same contact area with substrate but different contact angles, and droplet C has the same contact angle as the droplet B but a smaller contact area. The spatial scales are in millimeters.

Droplets B and C were found to show the same propagation rate of the freezing point isotherm. This result was consistent with our theoretical analyses suggesting the delay in solidification in the experiments was most likely due to the geometrical constraint in the heat flow caused by the increase in contact angle.

As noted in the previous section, there is a disparity between the reported time of initiation of freezing from the experiments and the values predicted from the theoretical modeling mainly due to the use of constant temperature boundary condition to solve the energy equation. To understand the effect of varying temperature of the substrate, we have plotted the temperature of the liquid near the triple contact-line for Droplets A, B, and C with respect to time in Figure 8a using the simulation results. For Droplet A, the temperature of the liquid near the substrate decreased almost immediately by nearly 20 K and reached 263 K in less than 1 s. For droplets B and C, the contact line temperature decreased to 290 K, but then took an additional 20 s to cool down to the same degree of supercooling. These results are consistent with our theoretical analyses predicting a 17-fold increase in the onset of freezing for droplet on cold-weather penguin feather compared to glass substrate. As a side note, experiments showed that water does not freeze exactly at 273 K, and freezing usually happened well below that. In our simulations, we assumed that freezing happens 10° below the freezing point (∼263 K).

The same set of simulations were performed (Fig. 8) for droplet of volume of 5 μl on a surface with the measured contact angles of cold and warm-weather penguins, see Figure 3, to show the effect of contact angle on the solidification delay. The results showed a 2.5 times delay in the start of freezing on cold-weather penguin feather ($\theta = 120°$) compared to warm-weather penguin feather ($\theta = 100°$), which is in excellent agreement with our theoretical (2.5×) and experimental (2.1×) data.

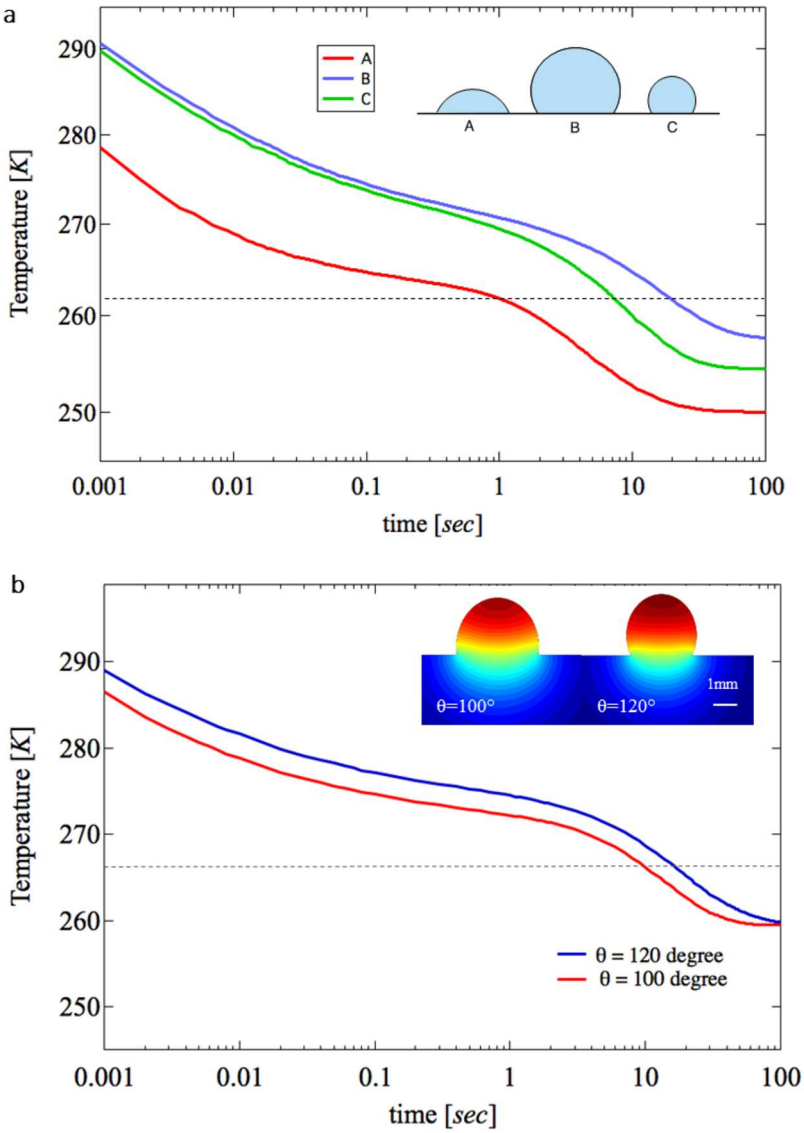

Fig. 8. Temperature at the trijunction. (a) Temperature variation with time at the trijunction for three water droplets at 300 K with different contact angles and contact areas on a surface with temperature at 250 K. The contact angle with the surface for these three droplets, starting from the left, are 70°, 120°, and 120° respectively. (b) Change in contact-line temperature with time for a droplet on warm-weather penguin $\theta = 100°$ and cold-weather penguin $\theta = 120°$. Dashed line shows the onset of freezing at triple contact-line.

7 Discussion and conclusion

This work was inspired by the examination of penguins in their natural habitat and the realization that penguins have the ability to completely prevent macroscopic ice formation on their feathers. Our investigations reveal that the anti-icing properties of penguin feathers are in large part due to the micro- and nano-porous surface texture of their feathers and the low critical surface tension of the preen oil covering them

make penguin feathers hydrophobic a property that is necessary but not sufficient. The freezing of the drops must be slow enough that drops cannot adhere to the feathers before rolling off.

An experimental and theoretical study was conducted to understand the solidification delay on both cold and warm-weather penguin feathers and the results were extrapolated to superhydrophobic surfaces in general. The results of experiments showed that transition from instantaneous freezing and large footprints to delayed solidification and less ice adhesion was possible using penguin feathers with cold water feathers delaying ice formation by approximately sixty times compared to a smooth surface and two times compared to a less hydrophobic, warm-weather penguin feathers. The freezing times were found to directly correlate to the static contact angle of the feather. Inspired by this observation, a theoretical model was developed to explain the heat transfer delay with increasing in contact angle on any generic water repellent surfaces, penguin feather or man-made superhydrophobic surface. Our theoretical analysis and numerical simulation results confirm that, for higher-contact-angle droplets, the inception of freezing was delayed. There are, however, other factors that can contribute to the icephobicity of a surface including the insulting air layer beneath the droplet and the scarcity of nucleation sites on the surface amongst others, although it is our contention that those effects are less substantial than the geometric delay presented here. The impact of these additional mechanisms were not included in this model, and the evaluation of their impact remains to be fully studied.

Supporting information available

The details of the gas chromatography/mass spectrometry (GC/MS) analysis of the preen oils covering the feathers and a simple set of numerical simulation performed to obtain the governing factors in the delay of ice formation as well as a discussion on the relative importance of each of these factors.

E.A.B. was financially supported by NSF grant CCF-1422795. J.P.R. would like to thank Abigail Rothstein for inspiring him to work on this project and for their many insightful conversations about penguins. We like to also thank Travis Moller for his help with GC/MS analysis.

References

1. Y. Le Maho, P. Delclitte, J. Chatonnet, Am. J. Physiol. **231**, 913 (1976)
2. J. Jacob, Syst. Ecol. **4**, 209 (1976)
3. W.C. Geer, J. Aeronaut. Sci. **6**, 451 (1939)
4. W.A. Cooper, et al., J. Aircraft **21**, 708 (1984)
5. R.W. Gent, N.P. Dart, J.T. Cansdale, Phil. Trans. R. Soc. A **358**, 2873 (2000)
6. Environmental Protection Agency, Effluent limitation guidelines and new source performance standards for the airport deicing category, 77 FR 29167, pp. 29167-29205, Document No 2012-10633, 2012
7. W.J. Jasinski, et al., Trans. ASME J. Solar Energy Eng. **120**, 60 (1998)
8. R. Carriveau, A. Edrisy, P. Cadieux, J. Adhes. Sci. Technol. **26**, 37 (2012)
9. N. Dalili, A. Edrisy, R. Carriveau, Renew Sustain Energy Rev. **13**, 428 (2007)

10. C.H.M. Machielsen, H.G.I. Kerschbaumer, Int. J. Refrig. **12**, 283 (1989)
11. M. He, et al., Soft Matter **6**, 2396 (2010)
12. M. He, et al., Soft Matter **7**, 3993 (2011)
13. L.L. Cao, et al., Langmuir **25**, 12444 (2009)
14. A.J. Meuler, G.H. Mckinley, R.E. Cohen, ACS Nano **4**, 7048 (2010)
15. L. Mishchenko, et al., ACS Nano **4**, 7699 (2010)
16. J. Lv, et al., ACS Nano **8**, 3152 (2014)
17. D.J. McCafferty, et al., Biol. Lett. **9**, 20121192 (2013)
18. K. Law, H. Zhao, *Surface wetting: characterization, contact angle, and fundamentals* (Springer, Switzerland, 2016)
19. D.M. Anderson, M.G. Worster, S.H. Davis, J. Cryst. Growth **163**, 329 (1996)
20. J. Robertson, C. Harkin, J. Govan, J. Forensic Sci. Soc. **24**, 85 (1984)
21. N. Du, et al., J. Theor. Biol. **248**, 727 (2007)
22. E. Bormashenko, et al., J. Colloid Interface Sci. **311**, 212 (2007)
23. E. Bormashenko, O. Gendelman, G. Whyman, Langmuir **28**, 14992 (2012)
24. S. Wang, et al., J. Phys. Chem. C **120**, 15923 (2016)
25. Y.K. Kamath, C.J. Dansizer, H.D. Weigmann, Soc. Cosmetic Chemists **28**, 273 (1977)
26. S. Srinivasan, et al., J. R. Soc. Interface **11**, 20140287 (2014)
27. J. Reneerkens, Functional aspects of seasonal variation in preen wax composition of sandpipers, PhD Thesis, University of Groningen, 2007
28. J.P. Rothstein, Annu. Rev. Fluid Mech. **42**, 89 (2010)
29. P.-G. de Gennes, F. Brochard-Wyart, D. Quere, *Capillary and wetting phenomena: drops, bubbles, pearls, waves* (Springer, New York, 2004)
30. K.Y. Li, et al., Langmuir **28**, 10749 (2012)
31. S. Jung, et al., Langmuir **27**, 3059 (2011)
32. E. Alizadeh-Birjandi, H.P. Kavehpour, J. Coat. Technol. Res. **14**, 1061 (2017)
33. T.M. Schutzius, et al., Langmuir **31**, 4807 (2015)
34. T. Maitra, et al., Langmuir **30**, 10855 (2014)
35. X. Sun, V.G. Damle, K. Rykaczewski, Adv. Mater. Interfaces **2**, 1400479 (2015)
36. P. Hao, C. Lv, X. Zhang, Appl. Phys. Lett. **104**, 111604 (2014)
37. M. He, et al., Appl. Phys. Lett. **98**, 162505 (2011)
38. H.F. Zhang, Y.Z. Rong Lv, C. Yang, Int. J. Thermal Sci. **202**, 59 (2016)
39. P. Tourkine, M. Le Merrer, D. Quere, Langmuir **25**, 7214 (2009)
40. A. Alizadeh, et al., Langmuir **28**, 3180 (2012)
41. D.M. Anderson, S.H. Davis, J. Fluid Mech. **268**, 34 (1994)
42. A.F. Mills, in *Heat transfer* (CRC Press, Homewood, Illinois, 1992), p. 888